Applied Mathematical Modelling 38 (2014) 2673–2688

Contents lists available at ScienceDirect

Applied Mathematical Modelling

journal homepage: www.elsevier.com/locate/apm

Transient finite element for in-bore analysis of 9 mm pistols

S. Deng [a], H.K. Sun [a], Chung-Jung Chiu [b,*], Kuei-Chi Chen [c]

[a] Department of Power Vehicle and System Engineering, Chung-Cheng Institute of Technology, National Defense University, Daxi Township, Tauyuan County 33551, Taiwan, ROC
[b] School of Defense Science, Chung-Cheng Institute of Technology, National Defense University, Daxi Township, Tauyuan County 33551, Taiwan, ROC
[c] Forensic Science Center of Military Police Command, Taiwan, ROC

ARTICLE INFO

Article history:
Received 25 October 2012
Received in revised form 3 September 2013
Accepted 11 October 2013
Available online 19 November 2013

Keywords:
In-bore process
Finite element method
Transient analysis

ABSTRACT

The in-bore process that occurs when a pistol is fired involves multiple physical models. This process is brief and typically measured in microseconds. Furthermore, propellants produce high temperatures and pressure gases during the burning process. These factors have made experimentation and simulation of the in-bore behavior of bullets difficult. This study uses a nonlinear transient finite element method (FEM) to simulate the in-bore behavior of a 9 mm bullet after being fired, where the chamber pressure is calculated by Vallier–Heydenreich formula and is used as the input loading. A gunshot experiment is conducted to verify the accuracy of computational results. The maximum difference between the numerical results and real experimental data is only 2.56% (including muzzle velocity and width and depth of engraved bullet vestiges), indicating that the simulation is credible.

The discussed simulation is capable of obtaining the plastic deformation and kinematic status of the bullet and the stress history and distribution of the gun barrel. The numerical results can provide complete data of the entire in-bore process, improve the drawbacks during real in-bore ballistic research experiments, and assist engineers in designing and developing other novel systems. The simulation can save considerable time when designing small arms barrels.

1. Introduction

Ballistics can be divided into interior ballistics, exterior ballistics, and terminal ballistics. Interior ballistics involves examining the chamber pressure, trajectory, and velocity of projectiles launched by propellants until outside the muzzle of a gun [1]. The interior ballistic theory can be used to estimate ballistic characteristics according to weapon system design parameters, or to design new weapon systems under specific conditions, such as muzzle velocities.

The in-bore process belongs to the field of interior ballistics. This process includes kinematics, solid mechanics, material science, fluid mechanics, heat transfer, and powder technology. These interactive physical models make in-bore research a complex topic. The brief action time, high temperature, and high-pressure gases make in-bore bullet behavior difficult to analyze. Ballistics research usually entails experimental tests requiring considerable manpower, materials, and time. The purpose of such tests is to derive empirical or semi-empirical formulas that can facilitate system design, manufacture, and operation. The drawbacks of real tests are the high cost, long development time, and the result may not be suitable for every system.

* Corresponding author. Address: No. 75, Shiyuan Rd., Daxi Township, Tauyuan County 33551, Taiwan, ROC. Tel.: +886 3 3809257; fax: +886 3 3906385.
E-mail address: c31020402@ndu.edu.tw (C.-J. Chiu).

0307-904X/$ - see front matter © 2013 Elsevier Inc. All rights reserved.
http://dx.doi.org/10.1016/j.apm.2013.10.071

For example, the width ratio of barrel rifling grooves and lands is approximately 1.5 in the United States, and ranges from 1.5 to 2 in Europe. The geometric (height and width) and numbers of rifling also have their own design empirical formulas. However, these geometric parameters calculated from empirical formulas and actually being used in production might up to several times in difference. Therefore, the design decisions depend significantly on experienced engineers.

Unlike traditional trial-and-error methods or, depending on the research modes of experienced engineers, computer-aided engineering (CAE) techniques have excellent numeric, visible, and reappearance attributes that can help engineers design and develop a new system efficiently. Today, CAE is accepted and widely used in many fields and has become an essential tool in contending with difficult measurement experiments and instantaneous reaction phenomenon analyses, such as those encountered in ballistics research.

In recent years, numerous research institutes and scholars have conducted experiments and numerical analyses on in-bore processes. Hopkins [2] evaluated the barrel dynamic stress at variable projectile velocities by coupling a gun interior ballistic model with the finite element software DYNA2D. He found that the dynamic peak stress of a M256 gun tube is 1.2 times higher than that of the static calculated result. Wilkerson and Hopkins [3] analyzed the dynamic motion of a gun tube during firing by considering the balanced breech design and mechanism clearance. Their research was applied to propose structural design improvements. Wilkerson [4] estimated the effects of the initial launch conditions on the kinetic energy projectile firing performance. The numerical model could explain the interaction between the projectile and the gun tube in detail. Rabern and Parker [5] applied finite element method (FEM) to improve the design of saboted launch packages. They modified the configuration of the launch packages to reduce the maximum operational stress caused by the launch load. Thus, the maximum muzzle velocity of the projectile could be raised from 1.9 km/s to 2.4 km/s and the penetration performance was increased. Chen [6,7] employed a 2D model to analyze the contact interaction between a rotating band and a projectile. He investigated the influence on contact pressure distribution using different material properties and discussed the deformation of elements. Russell [8] analyzed the interior of an M249 machine gun and the exterior ballistics (kinematics) using a 3D numerical model. A comparison between the numerical and experimental results showed a maximum inaccuracy of 6.91%. However, the detailed material parameters and initial/boundary conditions were not published. Kim et al. [9] investigated the deformation behavior of sabots and rods during launch with an unperfected straight gun tube and gravity load. They concluded that the curved path gun tube might considerably affect the lateral deformation of the projectile rod. South et al. [10–14] used a partially symmetric bullet/barrel model with simplified straight riflings to analyze the influence of material types, contact stiffness, and material viscosity on barrel radial stress. Furthermore, they executed several compression tests to estimate the behavior and suitability for new bullet materials. Vilkauskas [15] applied equivalent rifling methods that simplified a rifled barrel into a smooth barrel, and simulated an in-bore process using 2D and 3D symmetric models. He adjusted the equivalent frictional coefficient between the barrel and bullet to maintain consistency between the bullet's numerical and real test kinematic behavior, and can be applied to predict actual kinematic performance. Liu [16] set the projectile and barrel as rigid bodies, neglected the elastic and plastic behavior of materials, and discussed the influence of projectile mass eccentricity on interior ballistic kinematics. Ahmed et al. [17] simulated the dynamic response of a 120 mm gun barrel for off-axis masses after firing. The inertia force resulting from off-axis masses causes an additional barrel deflection. Sun [18] used 6 cm partial riflings and a projectile with constant base pressure, and calculated the rifling stress distribution during the firing process. Ge [19] compared the difference of projectile motion between smooth and rifled barrels. He showed that the riflings significantly affect the projectile behavior, and recommended that ballistic research should not neglect its influence. Liu and Fan [20] analyzed the barrel radial forging process based on the finite element analysis software DEFORM-2D. They built a simple 2D model and ignored the rifling structure. Their research demonstrated that the gun tube has compressive residual stress on the inner surface but tensile residual stress on the outer surface after radial forging. Chen [21] divided a rifle barrel into 50 ring sections and calculated the chamber pressure history of each section. Using this approach provides a more accurate simulation of barrel transient stress distribution. However, this approach only provided the concept of boundary condition setting without presenting any numerical results. Tao et al. [22] used an approximate formula to calculate the trend of engraving pressure under erosion and wear effects in the gun barrel. They showed that the variation in engraving pressure will change the ballistic performance (maximum chamber pressure and muzzle velocity) of the guns. Eches [23] set a 40 mm gun barrel as an elastic structure and the projectile as an elastic and plastic material. He developed a 3D numerical model to calculate the barrel's deformation and verified the result using real tests. Luo et al. [24] analyzed the limitation of frictional coefficient between the projectile positioning structure and internal barrel surface by static theoretical derivation and dynamic 2D numerical model simulation. Keinänen et al. [25] calculated the firing stress distribution of 2D gun tube models with different projectile rotating band geometries and material properties. They conjectured that the high firing stress of gun tubes plays a crucial role in fatigue failure, and plan to further investigate the topic by using a realistic 3D rifling model in their follow-up research.

Previous research has primarily focused on artillery and rifles, the majority of which provided a simplified analysis using a partial or 2D model. Some of the research did not include or even neglected the rifling effect during the launch process. Furthermore, several detailed numerical parameters and conditions remain unpublished. Therefore, this study develops a simple, efficient, and accurate process that can be applied to small-caliber systems with a full-sized 3D rifled barrel to calculate the kinetic in-bore barrel and bullet performance. In our previous exploratory study [26], the numerical result of a 5.56-mm rifle in-bore simulation was acceptable. This paper presents a simulation of a 9-mm pistol and a gunshot experiment to verify the numerical model. The result strengthens the verification and shows the reproducibility of the research process.

The primary numerical techniques employed using CAE are the finite element method, finite difference method (FDM), and boundary volume method (BEM). This research employs the FEM to simulate the in-bore behavior of a 9-mm pistol and uses solid elements to discretize the bullet/barrel model (Fig. 1). The Vallier–Heydenreich formula [27] is employed to calculate the input loading. An isotropic elastic–plastic with failure material type is adopted for all elements. Furthermore, this study also considers fractional effects and neglects air resistance and heat properties. When the simulation commences, the bullet is compressed by the loading pressure and propelled through the barrel in a spinning motion. Finally, shooting experiments were executed to verify the accuracy of the numerical model.

2. Theoretical foundation

2.1. Explicit dynamic analysis

We used the explicit dynamic finite element program, LS-DYNA, to solve the interior ballistics problems. The explicit method provides a suitable approach for shock behavior, stress wave propagation, and nonlinear problem research. By contrast, the implicit method is regularly used in static or vibration problems.

The governing equation of a dynamic system can be expressed as

$$M\ddot{U} + C\dot{U} + KU = F, \tag{1}$$

where M is the mass matrix; U, $\dot{U}$, and $\ddot{U}$ are the displacement, velocity, and acceleration vectors, respectively; C is the damping matrix; K is the stiffness matrix; and F is the loading vector.

The central difference method is used to solve time-domain transient problems. This method is attributed to explicit methods. Therefore, the central difference method is also called the explicit direct integration method. Assume U is nodal displacement; the velocity and acceleration at time t can then be expressed using the central difference method as

$$\dot{U}_t = (-U_{t-\Delta t} + U_{t+\Delta t})/2\Delta t, \tag{2}$$

$$\ddot{U}_t = (U_{t-\Delta t} - 2U_t + U_{t+\Delta t})/\Delta t^2, \tag{3}$$

where the subscripts indicate the time step, and Δt represents the time increment.

Substituting (2) and (3) into (1) yields

$$\hat{M}U_{t+\Delta t} = \hat{R}_t, \tag{4}$$

where $\hat{M} = M/\Delta t^2 + C/2\Delta t$ is the effective mass matrix, and $\hat{R}_t = F_t - (K - 2M/\Delta t^2)U_t - (M/\Delta t^2 - C/2\Delta t)U_{t-\Delta t}$ is the effective loading vector. From (4), displacement vector $U_{t+\Delta t}$ of next time moment $t + \Delta t$ can be obtained to determine the stress and strain [28].

2.2. Contact/impact algorithm

The penalty method is used widely to solve contact/impact problems. In this research, the relationships among the bullet, internal barrel surface, and bullet core and jacket are defined as contact-related.

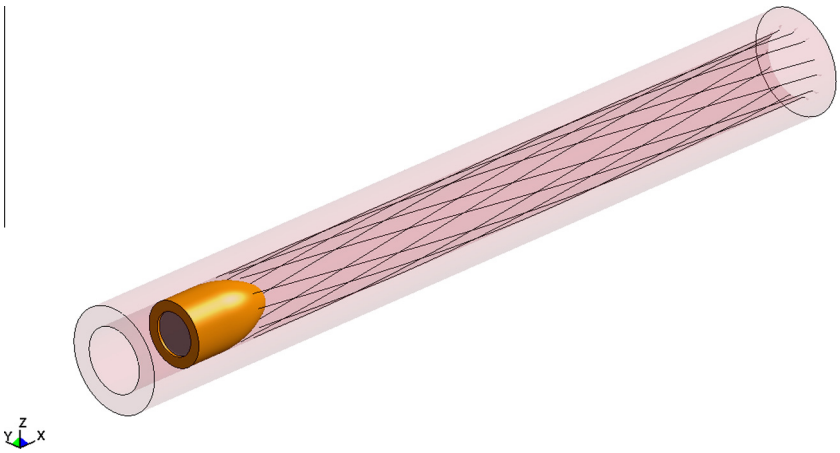

Fig. 1. Numerical model.

Assume that the surfaces of two objects are in contact with each other (master and slave surface). When penetration occurs within the contact pair, the penalty method adds nodal normal contact force to prevent penetration. The force is

$$f_s = -lk_i n_i, \tag{5}$$

where l is the distance of penetration. Penetration occurs when $l < 0$, whereas no penetration occurs when $l \geqslant 0$. k_i is the contact stiffness of the master surface element, and n_i is the unit normal vector of the master surface contact element. The penalty algorithm is not calculated if there is no penetration [28].

Eroding contact is a special contact case that implies the failure of one or both parts' contact material. When the strain or stress causes material failure, the element is deleted. The substratum material maintains its contact relation. This contact type can be used for failure research. According to the result of the gun shot experiment in this paper (Section 5), the bullet surface was observed to be engraved by rifling. Hence, we used the eroding contact between the bullet and the barrel to simulate the engraving phenomenon.

2.3. Elastic–plastic material model

The material is configured as isotropic elastic–plastic with failure. The deformation behavior consists of elastic and plastic regions according to von Mises criteria. In the elastic region, the material follows Hooke's law, and the relationship between stress and strain is linear. The slope E is Young's modulus. When unloading, the material obeys its elastic stress strain curve and returns to its initial state. Otherwise, when the equivalent stress $\bar{\sigma}$ equals yielding stress σ_y, then

$$S_{ij}S_{ij}/2 - \sigma_y^2/3 = 0 \tag{6}$$

and the material enters the plastic deformation phase. Here, $S_{ij} = \sigma_{ij} - \sigma_m\delta_{ij}$ is the deviatoric stress tensor, σ_m is the spherical stress or the hydrostatic stress, and δ_{ij} is the Kronecker delta. The stress–strain maintains a linear relationship, although the slope E_t differs from the elastic deformation phase. The relationships among tangent modulus E_t, plastic modulus E_p, and Young's modulus can be expressed as

$$1/E_t = 1/E + 1/E_p. \tag{7}$$

When unloading, the material has plastic strain ε_p (Fig. 2) [28,29].

3. Research procedure

This research is based on nonlinear FEM for ballistic analysis. The complete analysis process is introduced as follows: Step 1. Develop realistic virtual computer-aided design (CAD) models. The subsidiary parts and detailed geometric characteristics that do not affect the numerical results are neglected or simplified to reduce computation time; Step 2. Preprocess the numerical model, including define material types, mesh the model, and establish boundary conditions; Step 3. Solve the problem; Step 4. Post process and output data. This study uses the bullet's muzzle velocity and deformation as validation criteria to ensure the numerical model is accurate and rational. If the comparison between the numerical and real experi-

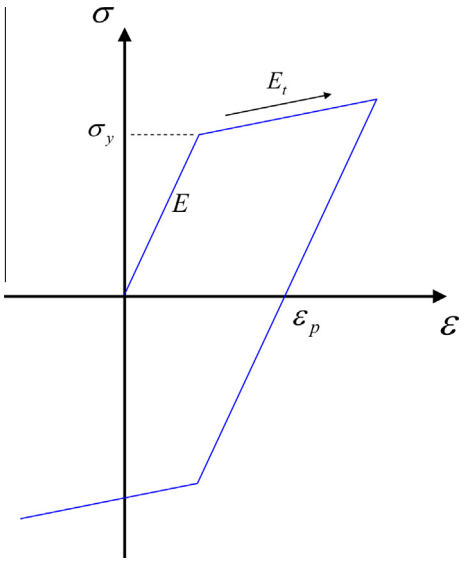

Fig. 2. Stress–strain relation of elastic plastic material.

ment results is inaccurate, then the model or boundary conditions should be examined and modified. The complete analysis process is shown in Fig. 3.

4. Numerical analysis

4.1. Pistol parameters

The 3D pistol model used in this study includes six dextral riflings. The basic parameters of the barrel and bullet are shown in Table 1.

4.2. FE model

The continuity of elements is highly essential for FE analysis. Only continuous elements can successfully transmit stress in structures. Using mapped mesh with 2D quad or 3D hexahedral elements can reduce the quantity of elements, improve solution precision, and decrease computation time. To discretize structures with continuous elements, the limitation of mapped mesh is higher than that of free mesh types. Hence, models with complex geometry are typically difficult to design and should be pre-planned using a mapped mesh type before discretization. The difference in limitations between free mesh models that use 2D triangle or 3D tetrahedral elements is relatively fewer, although free mesh increases the element quantity and computation time.

The model geometry is simple and easy to mesh with basic meshing techniques if only the riflings or barrel tube are considered. However, when the barrel is combined with 3D riflings, researchers are frequently forced to discretize the model using the free mesh method because of element continuity limitations. The expenses of the free mesh approach are increased element quantities and longer computation time. Moreover, the twist angle between riflings and barrels is narrow, and free mesh might produce illness elements with narrow angle near the border between riflings and barrel tube. These poor-quality elements might cause the FE program to be unable to converge and fail the analysis. Hence, using 2D plane or 3D symmetric models with smooth barrel or straight riflings are simple and widely used methods for interior ballistics research.

Generally, irrespective of whether using the 2D or 3D symmetric model is different from the real in-bore status, it cannot reach the full model visible purpose. Hence, this study built a 3D full-size rifled barrel, and planed the grid before discretizing the structure (Figs. 4 and 5). The purpose of grid planning is to define the mapped mesh, control and improve the quality of elements, and decrease the element quantities. Although it increases the building time of numerical models in this manner, the process can improve the velocity analysis and economize the calculation time. The overall effect is still worth using the mapped mesh types.

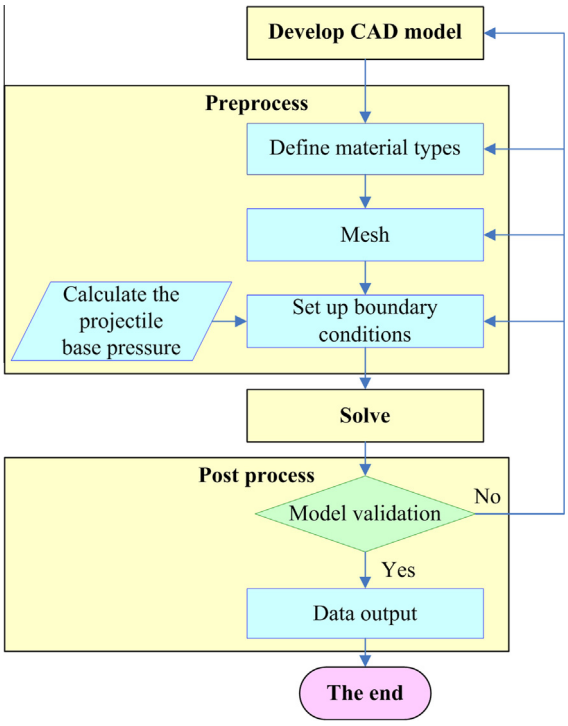

Fig. 3. Analysis process.

Table 1
Pistol parameters.

Target	Items	Parameters
9 mm pistol	Caliber (mm)	9
	Length of barrel (mm)	98
	Muzzle velocity (m/s) (measured from experiments)	350
	Quantity of riflings	6
	Mass of propellant (g)	0.325
	Mass of bullets (g)	9.45

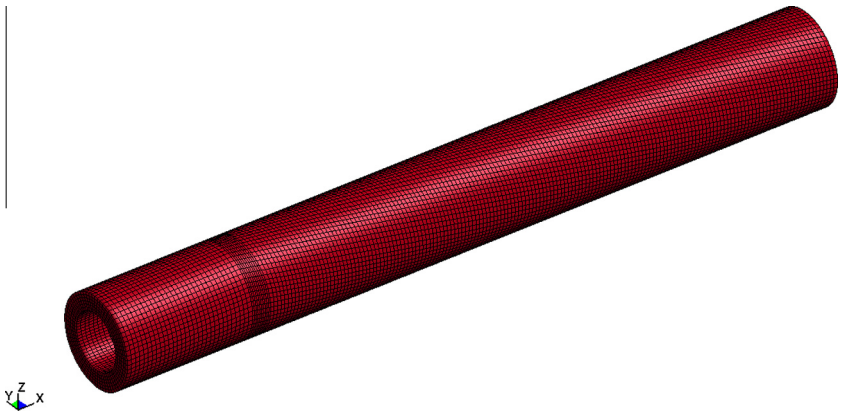

Fig. 4. The barrel FE model (Side View).

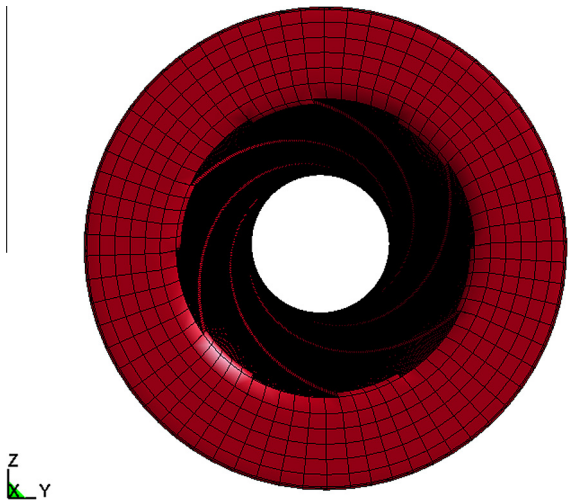

Fig. 5. The barrel FE model (Front View).

For example, a free mesh barrel is composed of 482 049 tetrahedral elements, and 188 elements are poor-quality elements, whereas a mapped mesh barrel is composed of only 84 300 hexahedral elements in the same mesh scale (a total reduction of 397 749 or 82.5% elements), and each element is a high-quality element (Table 2). Hence, we use mapped mesh to discretize the key structures in this research.

Regarding the finite element model of bullet, the copper alloy jacket and lead antimony alloy core of the bullet consist of 40 766 and 38 911 solid elements, respectively (Fig. 6).

4.3. Boundary conditions

The average chamber pressure history can be assessed according to specific parameters such as barrel length, bullet types, and propellant mass, by using the Vallier–Heydenreich empirical formula. The chamber gas pressure is not uniform, whereas

Table 2
Comparison of barrel element quantity using different mesh types.

Items	Barrel	
Mesh type	Free mesh	Mapped mesh
Element type	Tetrahedron	Hexahedral
Element quantity	482 049	84 300
Poor quality element quantity	188	0
Element quantity difference	−397 749 (−82.5%)	

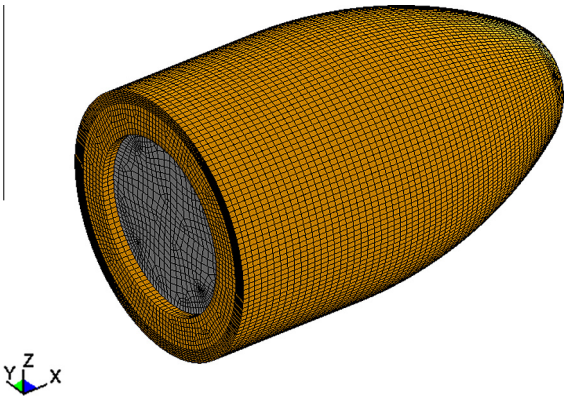

Fig. 6. The bullet FE model.

the chamber base gas has the lowest average velocity but a higher pressure level. Conversely, the projectile base gas trails the bullet and with a higher velocity but lower pressure. The relationship between projectile base pressure p_D and average chamber pressure p is

$$p = (1 + m_y/3\varphi_1 m_D)p_D, \tag{8}$$

where m_y is the propellant mass, m_D is the bullet mass, and φ_1 is the bullet mass coefficient [30]. In this research, the projectile base pressure is 98.9% of the average pressure from (8). Additionally, this analysis did not consider the primer time to reduce the analysis time. The projectile base pressure history in this case is shown as Fig. 7.

Reasonable initial and boundary conditions such as fixing, loading, and contact are set according to the pistol's operation principle. For example, the rear portions of the barrel are fixed to prevent motion; the back face of the bullet is loaded with a time-dependent distribution force, which is computed from Formula (8) to simulate the chamber gas acting on the bullet. Between the jacket and core of the bullet is surface-to-surface contact. Finally, the relationship between the projectile's external surface and the barrel's internal surface is eroding contact. The static friction coefficient is set as 0.3, and the dynamic coefficient is 0.1 based on our practical experience.

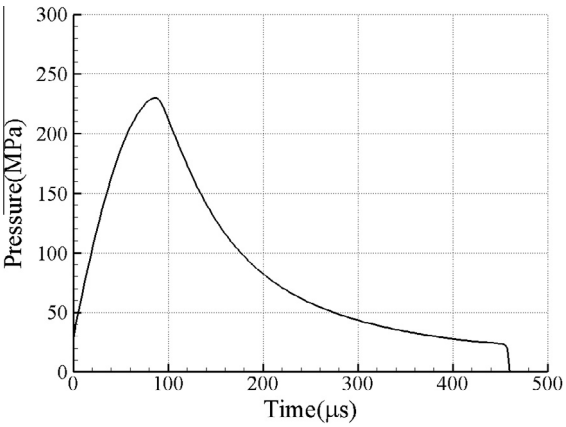

Fig. 7. Projectile base pressure time diagram.

4.4. Material parameters

The material type in this research is set to isotropic elastic–plastic with failure. The barrel is an AISI 4340 high-alloy steel and the bullet jacket and core is a UNS C22000 copper alloy and lead antimony alloy, respectively. The material parameters [31,32] details are presented in the Table 3.

5. Model validation

This study uses the muzzle velocity and bullet deformation as the validation criteria to ensure that the numerical model is correct and reasonable. The pistol's real test muzzle velocity is 350 m/s, whereas the calculated numerical result is 356.796 m/s (only 6.796 m/s or 1.94% difference).

The bullet is compressed and engraved as it passes through the barrel. When the bullet impacts against stony targets, it is liable to deform sharply and fragment into bits. The scale of impact deformation is much larger than the riflings' engraved effect. To obtain the bullet with complete riflings' engraved geometric characteristics, we shot toward a tank with filled water and used water as the deceleration medium. In this manner, we could obtain the bullet's integrity after being fired. Thereafter, by using micrograph and photo measurement techniques, we obtained geometric dimensions of the bullets' engraved vestiges.

This study measured and compared the width of engraved vestiges from real tests and numerical results (Figs. 8 and 9). Each group has 18 data (Table 4). The average width of the real test is 2.504 mm, with 0.045 mm standard deviation, whereas the average width of the numerical results is 2.462 mm, with 0.088 mm standard deviation. The difference between the real test and the numerical average data is 0.042 mm (or 1.68%).

Regarding the comparison of engraved vestiges' depth between real test and numerical results, each group has six data (Table 5). The average depth of the real test is 0.117 mm, with 0.005 mm standard deviation, whereas the average depth of the numerical results is 0.114 mm, with 0.042 mm standard deviation. The difference between the real test and numerical average data is 0.003 mm (or 2.56%).

This section shows the bullet's muzzle velocity; the engraved vestiges' width and depth are consistent for both experiment and simulation. The maximum difference is only 2.56%. This comparison indicates that the simulation is credible.

6. Result analysis and discussion

In the previous section, the correctness of the numerical model is checked. Hence, this study simulates in-bore kinetic motions and transient stress behavior based on this model. These factors are essential parameters for small arms design. Using real experimental tests is expensive and often can only obtain local area or specific moment data. Conversely, using the simulation employed in this study can yield the entire data of the overall process.

6.1. Bullet kinematic analysis

The numerical simulation shows us that the bullet is pushed forward by the chamber pressure to move along the barrel's axis. The projectile is compressed causing plastic deformation and guided to spin by riflings. The curve displayed in Fig. 10 shows that the bullet movement is miniscule (<1 mm) for the initial 51 μs because of inertial effects before increasing steadily. The traveling time of the projectile from a static position to being outside the muzzle is 456 μs (This research does not consider the primer time).

The analysis indicates that the bullet accelerates during the initial period after firing, although the rate of acceleration diminishes after 87 μs because of a reduction in base pressure. However, the bullet remains in a state of acceleration until it is outside of the muzzle. Finally, the velocity remains steady because air resistance is ignored in this simulation.

Fig. 11 is the acceleration history of the bullet. The rate of acceleration is significantly dependent on the projectile base pressure. The highest value of acceleration is 2.096×10^5 g at 87 μs. When the bullet is outside of the barrel, the materials lose lecture constriction and spring back sharply, causing the projectile to vibrate. This vibration diminishes over time.

Table 3
Listing of material parameters.

Items	Parts		
	Barrel	Bullet	
		Jacket	Core
Material type	AISI 4340 steel	UNS C22000 copper alloy	Lead antimony alloy
Density (g/cm^3)	7.85	8.8	11.04
Shear modulus (Gpa)	80	44	4.93
Yield stress (MPa)	1165	83	34
Plastic modulus (MPa)	1980	394	21
Bulk modulus (Gpa)	156.19	99.3	29.17

Fig. 8. Deformed bullet after shooting by real shot (marked region is the engraved vestige by riflings).

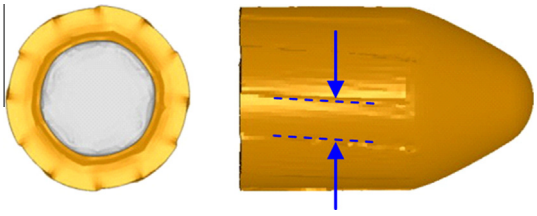

Fig. 9. Deformed bullet after shooting by numerical simulation (marked region is the engraved vestige by riflings, left part is bottom view of the bullet).

Table 4
Listing of engraved vestiges' width data.

Items	Data (unit: mm)			
Experiment	2.442	2.442	2.460	2.531
	2.496	2.566	2.460	2.549
	2.513	2.513	2.531	2.549
	2.549	2.504	2.540	2.549
	2.434	2.442	–	–
	Average: 2.504			
	Standard deviation: 0.045			
Simulation	2.449	2.271	2.521	2.469
	2.411	2.456	2.459	2.486
	2.448	2.427	2.504	2.610
	2.283	2.462	2.435	2.472
	2.540	2.618	–	–
	Average: 2.462			
	Standard deviation: 0.088			

Table 5
Listing of engraved vestiges' depth data.

Items	Data (unit: mm)			
Experiment	0.114	0.124	0.114	0.121
	0.121	0.112	–	–
	Average: 0.117			
	Standard deviation: 0.005			
Simulation	0.117	0.113	0.113	0.115
	0.110	0.113	–	–
	Average: 0.114			
	Standard deviation: 0.002			

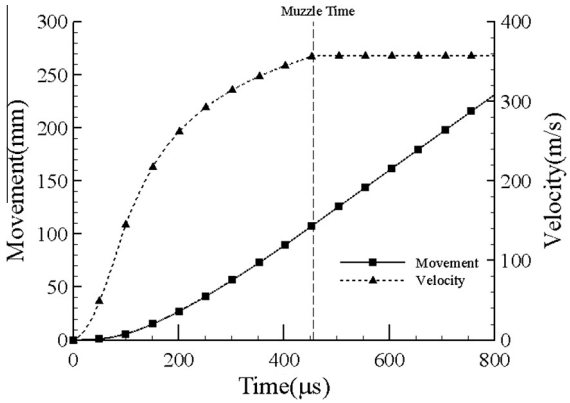

Fig. 10. Bullet movement and velocity curve.

Spin velocity is another crucial parameter for exterior ballistics because it affects projectile stability and flight dynamics. The angular velocity history diagram of the bullet (Fig. 12) shows that the projectile moves without rotation through the smooth-bore section. The spin-rate increases rapidly when the bullet slides into the rifling section at 84 μs. Therefore, a suitable smooth-bore distance design is crucial to reduce the torque effect. The rotational speed is corrected by riflings due to over rotating phenomenon in the beginning of rifling section, and then increased steadily until the bullet exits the muzzle. Finally, the rotational speed does not change obviously during free flight, and the value is 82 500.9 rpm. This phenomenon is difficult to replicate using experimental approaches. Conversely, one can analyze the full in-bore kinematic process of bullets by using this analysis.

6.2. Bullet' stresses analysis

The basic unit used to develop the numerical model for length, time, and mass is millimeter (mm), microsecond (μs), and gram (g), respectively. Hence, the unit of stress shown in the illustrations is tera Pascal (TPa). Fig. 13–17 show plots of the transient von Mises stress distribution of the bullet at different time during motion. The boat tail region and lecture section that contact the riflings are considered high stress zones during shot travel. High stresses in the rear region are caused by geometric stress concentration. The high lecture part stress is caused by the bullet being compressed by the riflings, which induces plastic deformation or failure. The material spring back effect creates the peak stress when the bullet exits the muzzle. The residual stress tends to decrease and stabilize over time. This analysis can be applied to future projectile design and material selection research.

6.3. Rifling' stresses analysis

Efficient rifling design can improve the performance and durability of small arms. These abilities depend highly on the stress distribution of riflings. Relevant theoretical derivation for rifling stress calculation is complete if it only considers a single variable. However, if we comprehensively consider multiple variables, such as contact, friction, torque, and deforma-

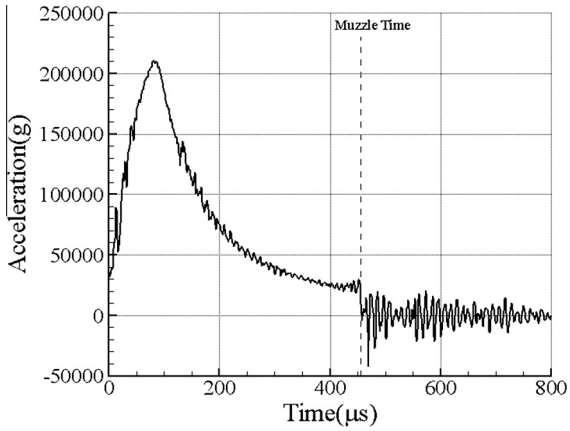

Fig. 11. Plot of the bullet acceleration curve (g = the acceleration of gravity).

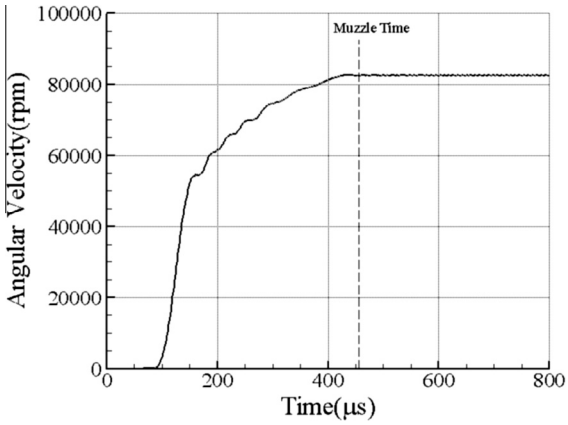

Fig. 12. Plot of the bullet spin curve.

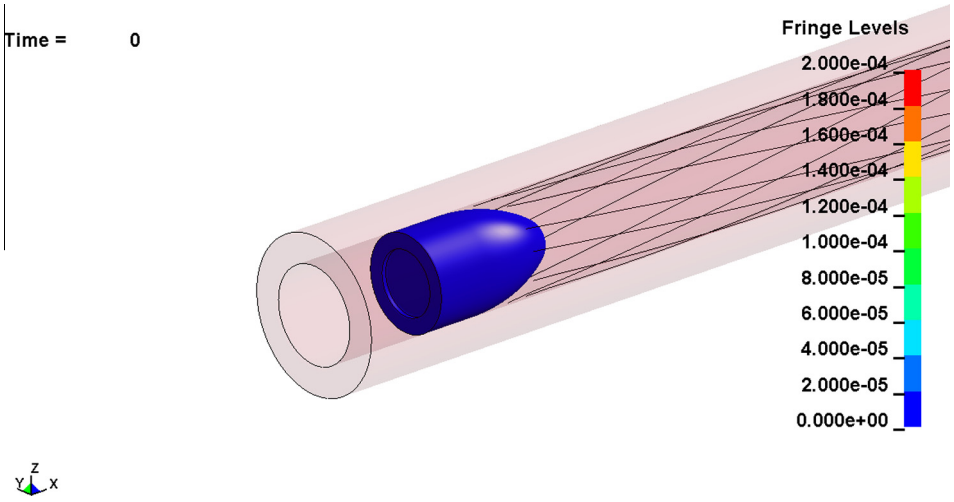

Fig. 13. Bullet stress distribution at time 0.

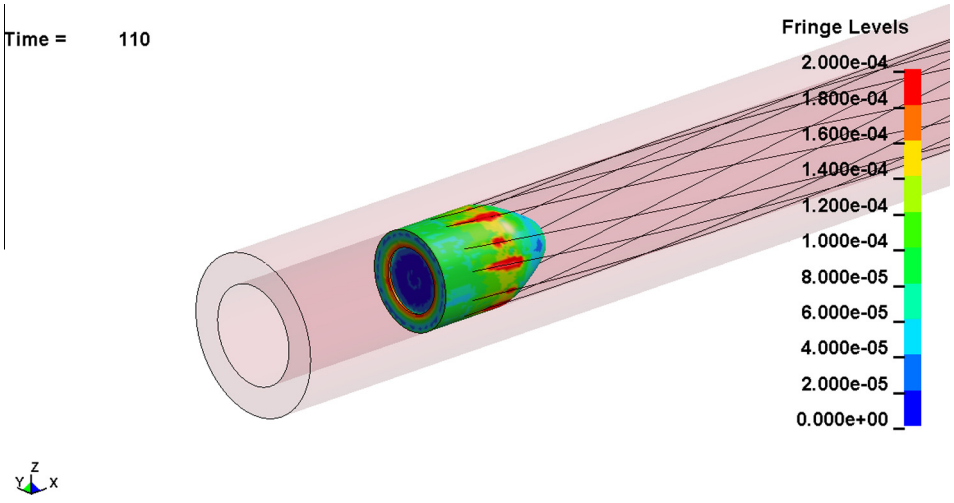

Fig. 14. Bullet stress distribution at time 110 μs.

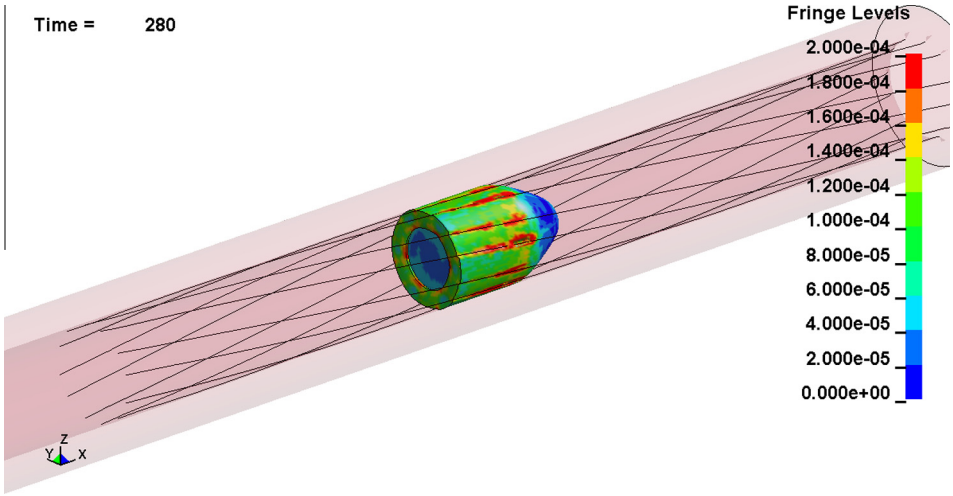

Fig. 15. Bullet stress distribution at time 280 μs.

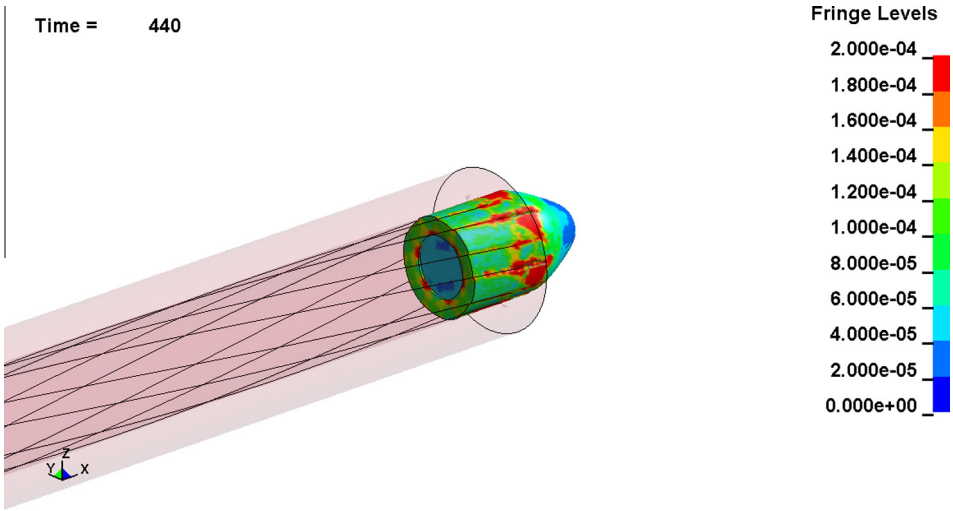

Fig. 16. Bullet stress distribution at time 440 μs.

tion, the topic becomes highly complex and problematic. Researchers frequently require the assistance of numerical computation to obtain the details of key structure stresses.

This paragraph details the transverse and longitudinal stress distribution on the rifling surface. Three transverse and equidistant nodal points (A, B, and C) on the rifling's surface element are selected (Fig. 18). Fig. 19 shows the stress curves diagram. The left regions on the land surface have higher stress levels, and the peak of instantaneous stress is 886.78 MPa. Conversely, the stress of the medium and right regions is relatively lower. The discussed pistol is a dextral rifled small arm. Its geometry shows that the bullet first contacts and compresses the rifling' left region while moving forward after being fired. Although Points B and C are then also compressed by the bullet, they do not directly cause the bullet to spin. This is why Point A has the highest instantaneous stress. The stress sequence also supports the geometric relationship.

Points A′, B′, and C′ are surface nodal points at the smooth, oblique, and contour sections of the land, respectively (Fig. 20). Fig. 21 shows the stress curve diagram. The results indicate that the stress depends highly on the contact sequence. The bullet contacts Point A′ first, and this stress occurs the earliest, followed by Points B′ and C′. The stress sequences are in accordance with the shooting process. Because Point A′ is at the smooth section without riflings, the interference between the land and the bullet is insignificant. Therefore, the land stress is at a minimum when the bullet passes this point. Point B′ is located at the initial region of the land surface and is directly impacted and compressed by the bullet. It has the highest stress level with a peak value of 634.1 MPa. At Point C′, the bullet has been engraved and is subsequently guided to spin along the riflings. The land's maximum stress is less than Point B′, with an instantaneous peak value of 429.56 MPa. In addition, the instantaneous stresses of barrel and the residual stresses of lands are high after the bullet travels through the barrel. This shows that the internal surface treatment of the gun barrel is extremely important (Fig. 22).

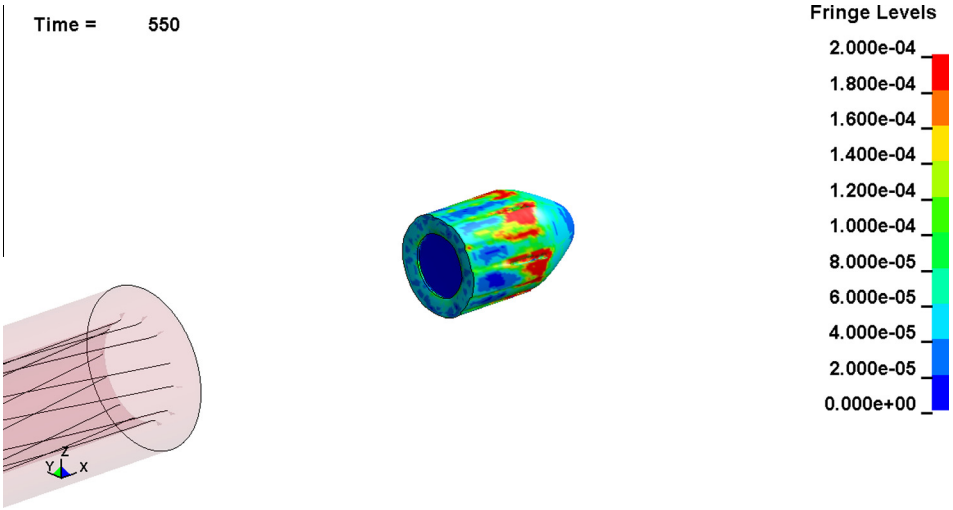

Fig. 17. Bullet stress distribution at time 550 μs.

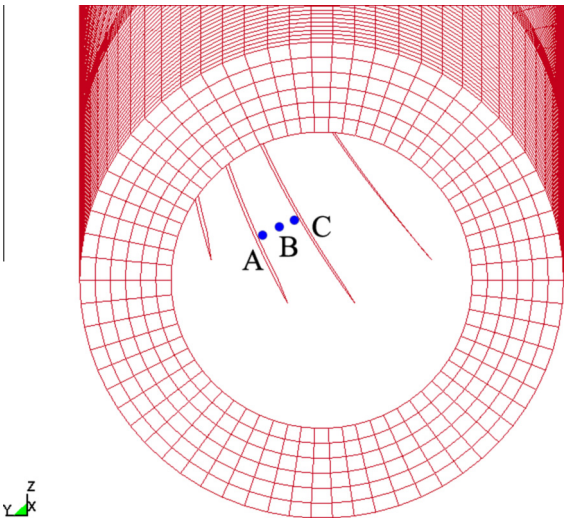

Fig. 18. Transverse nodal points' position on the land surface.

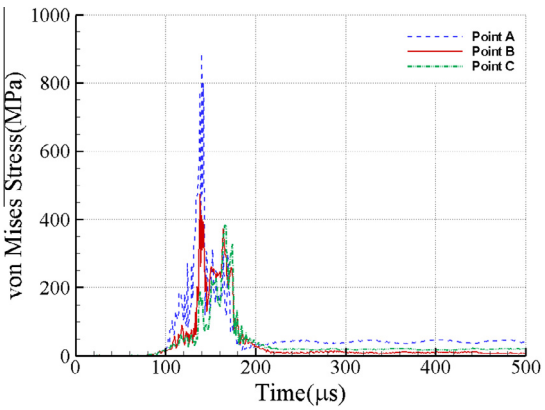

Fig. 19. Transverse nodal points' stress curves.

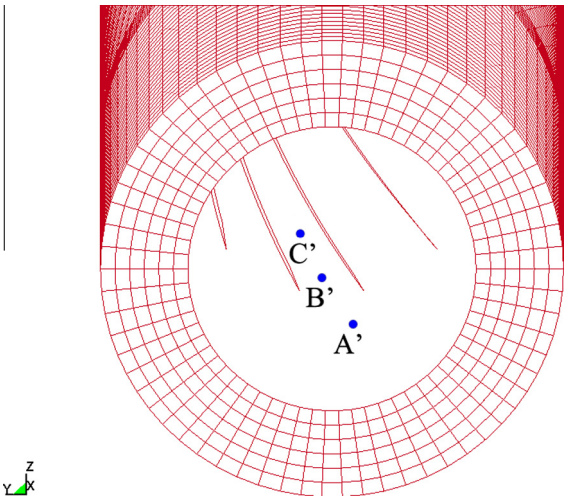

Fig. 20. Position of longitudinal nodal points on the land surface.

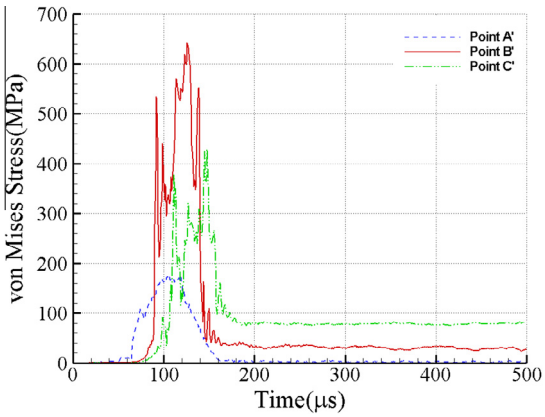

Fig. 21. Stress curves for the longitudinal nodal points.

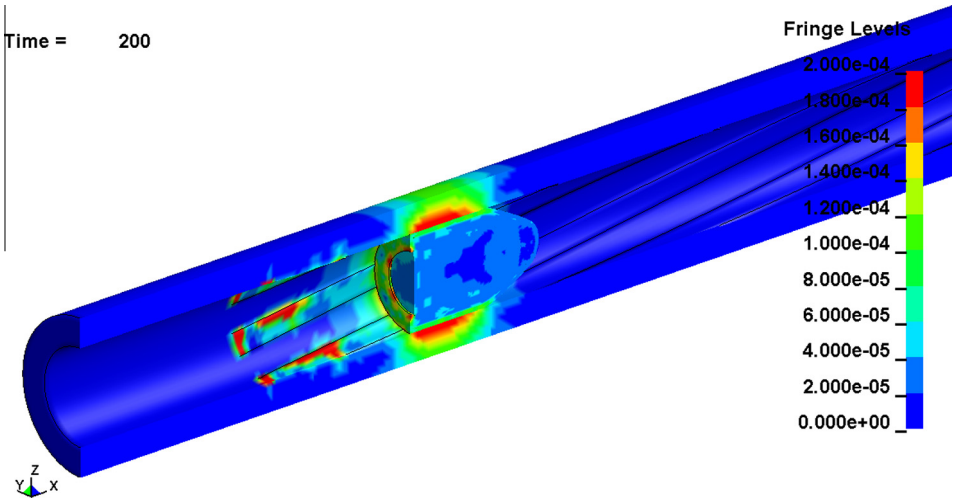

Fig. 22. Instantaneous stress and residual stress distribution at time 200 μs (the front half of the model is removed to show the in-bore stress).

7. Conclusion

The in-bore process of pistols is a multidimensional and complex topic. The relevant variables are numerous, and it is highly difficult to analyze using theoretical derivation. Even today, ballistics research requires considerable experimental tests.

This study uses a nonlinear transient FEM to simulate the in-bore behavior of a 9 mm pistol bullet after being fired. The research develops a realistic virtual rifled barrel/bullet model. The barrel included 3D riflings, and the bullet is composed of a core and jacket. Furthermore, a gunshot experiment is conducted to validate the accuracy of the numerical model. The maximum difference among the numerical results, including the muzzle velocity, the width and depth of engraved vestiges of the bullet, and real experimental data, is only 2.56%, indicating that the simulation is credible.

This simulation allows the collection of data for the whole shot travel, including movement, velocity, acceleration, rotation, stress, and strain. The kinematic analysis shows that the bullet's kinesis is the interaction with its base pressure, inertia, contact, deformation, and failure. Furthermore, bullet stress research is useful for projectile design and material selection. The rifling's stress shows that the stress distribution is relative to its location. For dextral rifling, the left side instantaneous maximum stress is higher than the right side of the land. At the initial land region, the oblique section has higher stress than the smooth and contour sections as the bullet passes through the rifled section. The high instantaneous and residual stress of the lands shows that the internal surface treatment of gun barrels is essential.

These useful and essential data are difficult to obtain through real experiments. However, in this research we applied nonlinear FEM to obtain the complete data. The simulation of this research can save significant amounts of time for design barrels of small arms.

In order to simplify the numerical model and reduce computation time, this study neglects the heat effects. Heat produced by propellant and friction could affect the stresses of barrel. It is necessary to analyze the heat effect deeply, and this will be considered in the future work.

Acknowledgment

The authors would like to thank the National Science Council, Taiwan, for their financial support (Project No. NSC 100-2221-E-606-008).

References

[1] D.E. Carlucci, S.S. Jacobson, Ballistics: Theory and Design of Guns and Ammunition, CRC Press, Boca Raton, 2008.
[2] D.A. Hopkins, Predicting dynamic strain amplification by coupling a finite element structural analysis code with a gun interior ballistic code, Technical report No. BRL-TR-3269, U.S. Army Laboratory Command, 1991.
[3] S.A. Wilkerson, D.A. Hopkins, Analysis of a balanced breech system for the M1A1 main gun system using finite element techniques, Technical Report No. ARL-TR-608, US Army Research Laboratory, 1994.
[4] S.A. Wilkerson, The effect of initial and gun mount conditions on the accuracy of kinetic energy (KE) projectiles, Technical Report No. ARL-TR-895, US Army Research Laboratory, 1995.
[5] D.A. Rabern, R.B. Parker, Lunch behavior of 60-mm pushed and traction driven saboted launch packages, Int. J. Impact Eng. 16 (1) (1995) 133–148.
[6] P.C.T. Chen, Analysis of engraving and wear in a projectile rotating band, Technical report No. ARCCB-TR-99012, US Army Armament Research, Development and Engineering Center, 1999.
[7] P.C.T. Chen, M. Leach, Modeling of barrel/projectile interaction in a rotating band, Technical report No. ARCCB-TR-01011, US Army Armament Research, Development and Engineering Center, 2001.
[8] K. Russell, On dynamic non-linear finite element analysis of bullet and barrel interface, in: Joint services small arms section annual symposium, exhibition, firing demonstration and plant tour, Kansas City, MO, 2003
[9] J.B. Kim, M.G. Kim, Analysis for material behavior of sabot/rods during launch by finite element method, Int. J. Mod. Phys. B. 17 (2003) 1884–1890.
[10] J. South, J. Newill, D. Kamdar, J. Middleton, F. Hanzl, G. DeRosa, Bridging the gap between the art and science of materials for small caliber ammunition, AMPTIAC Quart. 8 (4) (2004) 57–63.
[11] J. South, A. Yiournas, M. Minnicino, The effect of slug material on the behavior of small-caliber ammunition, Technical report No. ARL-TR-3901, Aberdeen proving Ground, MD, US Army Research Laboratory, 2006.
[12] J. South, B. Power, M. Minnicino, Evaluations of computational techniques for the engraving of projectiles, in: Computational Ballistics III, WIT Transactions on Modelling and Simulation, vol. 45, 2007, pp. 193–202.
[13] J. South, D. Kamdar, M. Minnicino, Small caliber modeling from design to manufacture to launch, in: 23rd International Symposium on Ballistics, Tarragona, Spain, 2007.
[14] J. South, A. Yiournas, J. Wagner, J. Brown, R. Kaste, A study of the engraving of the M855 5.56-mm projectile, Technical Report No. ARL-TR-4743, US Army Research Laboratory, 2009.
[15] A. Vilkauskas, Research and simulation of ballistics processes of small arms ammunition bullets, Summary of doctoral dissertation, Kaunas University of Technology, 2005.
[16] L. Liu, Y.S. Chen, G.L. Yang, A study on the projectile-barrel coupling based on contact model, Acta Armament. 27 (6) (2006) 984–987.
[17] N. Ahmed, R.D. Brown, A. Hameed, Finite element modelling and simulation of gun dynamics using 'ANSYS', in: Tenth International Conference on Computer Modeling and Simulation, 2008.
[18] H.Y. Sun, J.S. Ma, G.M. Zhang, B. Jin, Analysis of the land stress during the engraving process, J. Ordn. Eng. College 20 (4) (2008) 43–46.
[19] J.L. Ge, G.L. Yang, Y.S. Chen, W. Xu, A study on projectile-barrel coupling problem based on elastoplastic contact/impact model, J. Ballist. 20 (2008) 103–106.
[20] L. Liu, L. Fan, Study of residual stresses in the barrel processed by the radial forging, in: Proceedings of the 2009 Second International Conference on Information and Computing Science, IEEE Computer Society, vol. 4, 2009, pp. 131–134.
[21] M.M. Chen, High fidelity in-bore pressure modeling, in: 11th International LS-DYNA® Users Conference, Michigan, 2010.
[22] C. Tao, Y. Zhang, S. Li, C. Jia, Y. Li, X. Zhang, Z. He, Mechanism of interior ballistic peak phenomenon of guns and its effects, J. Appl. Mech. 77 (2010) 051405.

[23] N. Eches, D. Cosson, Q. Lambert, A. Langlet, J. Renard, Modeling of the dynamics of a 40 mm gun and ammunition system during firing, in: 26th International Symposium on Ballistics, Florida, 2011.
[24] Q. Luo, X. Zhang, Research for a projectile positioning structure for stacked projectile weapons, J. Appl. Mech. 78 (2011) 051015.
[25] H. Keinänen, S. Moilanen, J. Tervokoski, J. Toivola, Influence of rotating band construction on gun tube loading – Part I: numerical approach, J. Press. Vess. 134 (2012) 041006-1–041006-6.
[26] S. Deng, H.K. Sun, C.C. Chiu, Rifles in-bore finite element transient analysis, in: International Conference on Mechanical, Production and Materials Engineering, 2012, pp 58–62.
[27] Oerlikon Pocket Book, Oerlikon Machine Tool Works, 1958.
[28] J.O. Hallquist, LS-DYNA® Theory Manual, Livermore Software Technology Corporation, California, 2006.
[29] W.F. Chen, D.J. Han, Plasticity for Structural Engineers, Springer, New York, 1988.
[30] L. Jedlicka, S. Beer, M. Videnka, Modelling of pressure gradient in the space behind the projectile, in: Proceedings of the 7th WSEAS International Conference on System Science and Simulation in Engineering, WSEAS Press, 2008, pp. 100–104.
[31] MatWeb, <http://www.matweb.com/>.
[32] F. Habashi, Alloys: Preparation, Properties, Applications, Wiley-VCH, New York, 1998.